Adaptive Collision-Limitation Behavior for an Assistive Manipulator

Martin F. Stoelen, Virginia F. Tejada, Juan G. Victores, Alberto Jardón Huete,
Fabio Bonsignorio and Carlos Balaguer

Abstract— **Assistive robot manipulators aim to allow disabled users to perform physical Daily Life Activities (DLA) safely and effectively in environments with both unknown and dynamic elements. Here the approach taken is to aid the user by means of an adaptive shared control. A set of distributed collision and proximity sensors is used to aid in limiting collisions during direct control by the user. Artificial neural networks adapt the use of the proximity sensors online, which limits movements in the direction of an obstacle before a collision occurs. The system learns by associating the different proximity sensors to the collision sensors where collisions are detected. This enables the user and the robot to adapt simultaneously and in real-time, with the objective of converging on a usage of the proximity sensors that increases performance for a given user, robot implementation and task-set. The system was tested in a controlled setting with a simulated 5 DOF assistive manipulator and showed promising reductions in Mean Time (MT). It extends earlier work by showing the approach can be applied to full multi-link manipulators.**

I. INTRODUCTION

Assistive manipulators aim to increase the level of independence of its users through aiding in physical Daily Life Activities (DLA). One example is the commercial Exact Dynamics iArm, see Fig. 1(a). Another is ASIBOT, a 5 Degree Of Freedom (DOF) manipulator developed at Universidad Carlos III de Madrid (UC3M) [1]. See Fig. 1(b). Assistive manipulators typically require operation in close proximity to the disabled or elderly user and safety is therefore critical. They also aim to perform tasks in real-world unstructured environments such as a user's home. For a robot, autonomous or teleoperated by a potentially disabled user, reliably performing such tasks remains a challenge. One solution may be to enable both the user and the robot to use their own sensing, control and planning capabilities in a cooperative way. This is also known as shared control.

Vanacker et al. [2] presented a strategy for filtering the commands coming from the disabled user of a wheelchair using contextual information from sensor readings as well as previous data from able-bodied users. A more recent approach used plan recognition to obtain the probability of a set of user plans, given a set of observed user commands [3]. Another approach for predicting the intent of a wheelchair user was shown in [4], where specific local models for actions, for example moving towards a door, is used. There is also considerable work on mobile robots that have an adjustable degree of autonomy, for example by the user of the robot. Here shared control is on the lower end of the scale of potential autonomous modes. See for example [5].

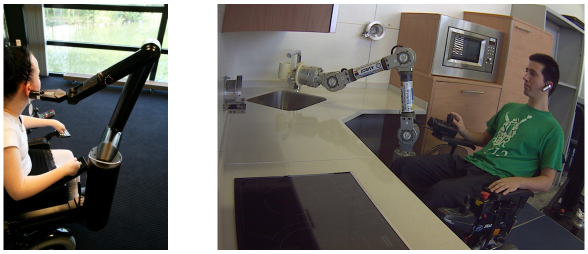

(a) The iArm. (b) ASIBOT in the UC3M kitchen test bed.

Fig. 1. Example assistive manipulators.

For higher-DOF platforms like manipulators there is less work available, although collaborative selection among known objects in the environment shows promise [6]. Given that accumulative errors around a few centimeters are likely the maximum that can be tolerated for manipulation, it may be beneficial to sample the state as directly as possible with proximity sensing. Thus taking out model-related errors and minimizing the information processing required. See for example previous work by the authors on an adaptive proximity-based collision-limitation behavior [7]. This is here developed further and extended to a complete assistive manipulator.

II. SYSTEM DESCRIPTION

A. Overview

The shared control described here uses a set of distributed collision and proximity sensors to limit collisions during direct control by the user. There are two principal contributions. First, it can be applied on high-DOF assistive manipulators sharing control with a user in a dynamic and partially unstructured environment. Second, the implemented system adapts the use of the proximity sensors online to a given user disability and task-set through an unsupervised Hebbian learning. This allows the robot and user to mutually adapt to each other, giving the user continuous feedback on, and the ability to respond to, changes in the system.

B. Proximity Sensing

Both ultrasonic and infrared proximity sensors are common in mobile robotics. The latter have also been previously

Martin F. Stoelen, Virginia F. Tejada, Juan G. Victores, Alberto Jardón Huete, and Carlos Balaguer are members of the RoboticsLab research group within the Department of Systems Engineering and Automation, Universidad Carlos III de Madrid (mstoelen, vtejada, jcgvicto, ajardon, balaguer)@ing.uc3m.es

Fabio Bonsignorio is a member of the RoboticsLab as Santander Chair of Excellence in Robotics at Universidad Carlos III de Madrid and CEO/founder of Heron Robots of Genova, Italy bonsign@ing.uc3m.es

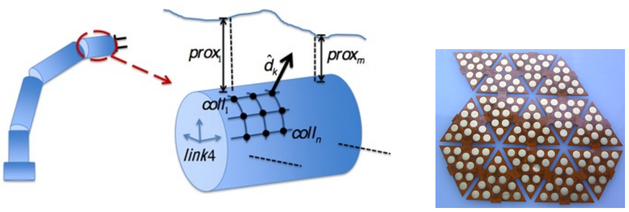

(a) For each robot link; n collision sensors (grid), m proximity sensors (dotted lines).

(b) Example of existing tactile sensors, from [8].

Fig. 2. Collision and proximity sensing assumed for approach.

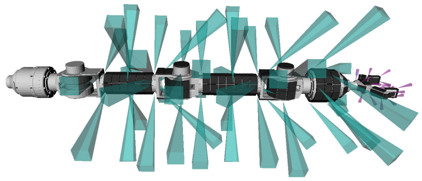

Fig. 3. Collision sensors (black squares) and proximity sensors implemented on the virtual ASIBOT manipulator. Simulated field of view shown for each proximity sensor: Medium-range Sharp GP2D120 and short-range Vishay TCND5000 as green and purple square pyramids, respectively.

used in full-body proximity sensing on robot manipulators [9], and for grasping [10]. In general m infrared proximity sensors and n discrete collision sensors are here assumed for each link of the robot manipulator, see Fig. 2(a). Any type of proximity sensor can be used however, even a mix of different types for redundancy. The final implementation had 68 proximity sensors in total. See Fig. 3. 18 were simulated as Vishay TCND5000 (maximum distance 50 mm). These were all distributed over the end-effector. The remaining sensors were simulated as Sharp GP2D120 (maximum distance 400 mm). All proximity sensors had a simulated 10° field of view, represented in the simulation by a square 6 by 6 array of point distance measurements. The lowest of the 36 point distance measurements was used at any time. The voltage output of each proximity sensor, p_j, was simulated based on the distance measured, $prox_j$, and the calibration specifications of the different sensor types. See Fig. 4. That is, the signal used by the neural network varied inversely to the distance measured (in the nominal range of the sensor).

C. Collision Sensing

There is currently a large research effort focused on developing tactile sensing for robots. See for example Fig. 2(b). For the simple collision sensing used here, the assumed minimum spatial resolution of the tactile sensing was 20 mm, which is well within the capability of the current state of the art [11]. See Fig. 3. A discrete value was used to represent the existence of a collision for each collision sensor. The total number of individually distinguishable collision sensors simulated for the manipulator was 229.

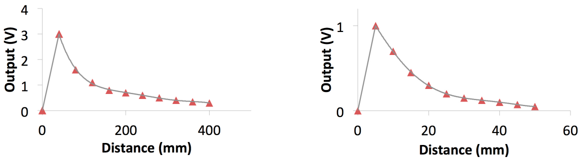

(a) Sharp GP2D120.

(b) Vishay TCND5000.

Fig. 4. Plots of simulated voltage output for proximity sensors used (p_j). Gray line is output assumed, red triangles are calibration data points.

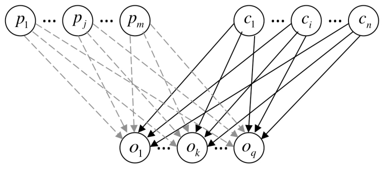

Fig. 5. Artificial neural network with discounted Hebbian learning for m proximity sensors (dashed grey arrows are synapses), p_j, and fixed weights for n collision sensors (solid black arrows are synapses), c_i.

D. Adaptation of Proximity Sensor Usage

The addition of a collision-limitation behavior can potentially affect negatively both the performance and satisfaction of the user. It would therefore be beneficial for the system to apply the minimum required amount of assistance for a user's abilities and disabilities, while maximizing the overall performance. An adaptation of the use of the proximity sensing to each user may help achieve this goal, which should preferably be performed online to make sure the user can keep up with, and respond to, the changes in the system. Virtual proximity sensors with a known location and pose are defined a priori ($\widehat{d_k}$ in Fig. 2(a)). Learning is then used to relate the actual proximity sensors to these virtual sensors. A Hebbian learning approach was chosen, inspired by the Distributed Adaptive Control (DAC) paradigm for autonomous robots [12]. See Fig. 5. Each collision sensor is hardwired (weight initialized offline) to one virtual sensor, and they were therefore here assumed to be collocated. The activation of each of the neurons representing the virtual sensors, o_k, was made to vary linearly with the input to the respective neuron, according to Equation (1).

$$o_k = \sum_{i=1}^{n} w_{k,i} c_i + \sum_{j=1}^{m} w_{k,j} p_j. \tag{1}$$

The proximity sensors have full connectivity to the layer representing the virtual sensors, and the weights ($w_{k,j}$) are updated using the discounted Hebbian learning rule in Equation (2). Learning occurs whenever there is input from a given collision and proximity sensor, while "forgetting" (the discounting over time) occurs at all times. The relative strength of these two processes are controlled with the learning rate η and discount rate ϵ, respectively. The parameter γ can be used to control the rate of change of the weights in general. The corresponding fixed weights and the parameters η and ϵ are tuned to avoid learning with only proximity input. See Fig. 6 for an example of the learned neural network weights for one link.

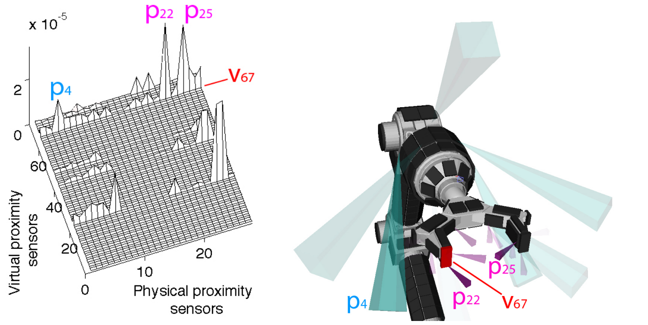

(a) Neural network weights. (b) Corresponding visualization for v_{67}.

Fig. 6. Example neural network weights for final link (participant 5 in experiment). Visualization of weights for one virtual proximity sensor shown (v_{67}). Transparency of square pyramid representing the field of view of a given physical proximity sensor is made to vary with the corresponding weight connecting it to v_{67}. High transparency indicates low weight.

$$\Delta w_{k,j} = \frac{\gamma}{m}(\eta o_k p_j - \epsilon w_{k,j}). \tag{2}$$

E. The Proximity Ratio

Algorithm 1 shows the scheme used for calculating the maximum proximity ratio for each link. Each virtual sensor “reading” $\vec{d_k}$ is given the magnitude of the inverse of the respective output of the neural network o_k. Then the “reading” that has the largest ratio of the projection of the commanded velocity and its own magnitude is used at each instant. This ratio is here named the proximity ratio r_k. The constant ξ_{vel} is chosen to be small to avoid computational issues if o_k is zero. The proximity ratio can then be used to limit velocities based on the virtual sensor “reading” where a collision will likely occur, and where collisions have occurred in the past (learned by the neural network). A non-zero α_{proj} means velocities in other directions are also slowed down. The translational velocity of each virtual sensor, $\vec{v_k}$, is deduced from the user's commanded velocity for the end-effector and the current kinematic pose of the robot. This is further described in section II-F.

Algorithm 1 Maximum proximity ratio for a link, based on the translational velocities of the virtual sensors, $\vec{v_k}$, the outputs of the link-specific neural network, o_k, and the direction of the respective virtual sensors, $\widehat{d_k}$.

```
for $k = 1$ to q do
    $\vec{d_k} = \frac{1}{o_k + \xi_{vel}} \widehat{d_k}$
    $proj_k = \vec{v_k} \cdot \widehat{d_k}$
    $r_k = \frac{\alpha_{proj} + \beta_{proj} proj_k}{||\vec{d_k}||}$
end for
$r_{max} = \max_k(r_k)$
```

F. Full-Body Collision-Limitation

Fig. 7 shows the schema for the collision-limitation behavior for a complete multi-link manipulator. The received velocities of the end-effector, $\vec{v}_{ee}$, are here represented in the robot base frame (b superscript). Using an iterative solver for the inverse Jacobian, the corresponding joint velocities for all joints are calculated. Then each link is treated separately. Using the known kinematic structure of the robot and the current joint angles, the translational velocities of each sensor for each link is calculated. These are then used together with the output of the link-specific neural network to produce the maximum proximity ratio for that link, as described in section II-E. The learning is thus spread over multiple instances of neural networks, each running independently. Finally, the original commanded end-effector velocities are limited based on the maximum proximity ratio for the complete manipulator. The output velocity, $\vec{v}_{ee,out}$, is the user-commanded velocity $\vec{v}_{ee}$ divided by this ratio. The behavior will only activate if the ratio exceeds one. This enables the limitation of velocity based on the learned virtual sensor usage of the complete manipulator. Audio feedback was used to help the user assess when the collision-limitation behavior was acting. This consisted of simple tones being played with breaks in between. The frequency of the alternation was proportional to the current maximum proximity ratio, see Fig. 7. The frequency of the tones was used to identify the link, from low frequency at the base to high frequency at the end-effector.

III. EXPERIMENT METHOD

A. Participants

8 able-bodied participants were used, all graduate and under-graduate students at UC3M. There were 3 female and 5 male, all right-handed. 4 had previous experience with 3D input devices and 3 had previous experience controlling robots. The mean age was 23.7, with a range from 19 to 40. Each participant was paid €10 for participation.

B. Simulated Disability

As in previous work by the same authors [7], a noise was added to the user input, according to Equation (3). This was Gaussian noise, low-pass filtered at 2 Hz and generated independently for each Cartesian component of the noise vector ($\vec{z} = [z_x, z_z, z_{pitch}, z_{yaw}]^T$). The magnitude of the translational velocities caused by the noise increased proportional to the magnitude of the translational velocities commanded by the user, with some noise existing also when the user did not indicate movement (non-zero α_{noise}). Similarly for the rotational velocities. See Fig. 8(b) for example trajectories.

$$\begin{aligned}
&\vec{v}_{ee} = \vec{v}_{input} + \vec{v}_{noise}, \\
&where: \\
&\vec{v} = [\vec{v}_{trans}, \vec{v}_{rot}]^T = [v_x, v_z, v_{pitch}, v_{yaw}]^T, \\
&and: \\
&\vec{v}_{noise,trans} = \vec{z}_{trans}(\alpha_{noise} + \beta_{noise}||\vec{v}_{input,trans}||), \\
&\vec{v}_{noise,rot} = \vec{z}_{rot}(\alpha_{noise} + \beta_{noise}||\vec{v}_{input,rot}||), \\
&z_x, z_z, z_{pitch}, z_{yaw} \sim \mathcal{N}(0, \sigma^2).
\end{aligned} \tag{3}$$

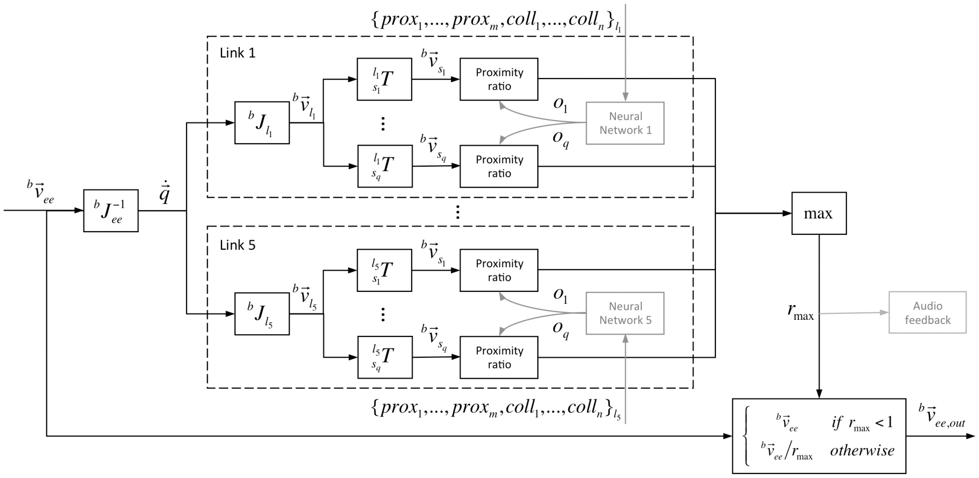

Fig. 7. The full-body collision limitation schema. The current joint angles are used in calculating the Jacobian, but are here omitted for clarity. The b superscript is used to denote the robot base frame. Grey color indicates external modules.

This served as a crude estimation for the loss of control caused by a physical impairment, and allowed for a homogeneous set of able-bodied participants. While real end-user participants are needed to validate the clinical credibility of any assistive technology [14], the use of simulated disabilities can help drive the early development. For example a random component being added to an able-bodied user's computer mouse movements [15]. Other exploratory works in shared control have also used simulated disabilities, for example the inability to move in a given direction [3]. A velocity-dependent noise was here used, as it amplifies an effect already seen in the speed-accuracy trade-off of many human movements. That is, faster movements require greater forces in the muscles, which again may introduce more nervous system noise [16]. An increase in the signal-dependent neuromotor noise has been related to stroke-related motor deficiencies [17], and children with dystonia (movement disorder that causes involuntary muscle contractions) [18].

C. Simulated Environment and Tasks

The simulated environment used in the experiment can be seen in Fig. 8. The experiment was performed in the OpenRAVE virtual environment [13], running at approx. 50 Hz. The ASIBOT robot was simulated to be attached to the right-hand side of the user's wheelchair. A view from behind the simulated user was given, to simulate the approximate size of the field of view that the participant would have sitting in the wheelchair. Implementing the system first in simulation provided a flexible and easily controllable environment for including human trials actively in the development process [7]. The tasks performed involved moving the end-effector of the robot from an initial resting position to a pre-grasp position around one of 5 simulated cans in the virtual environment. See Fig. 8(a). For a given trial the target can was red, while the remaining were blue. A trial was automatically judged as completed when the two fingers of the robot end-effector was positioned around the thickest part of the can, stopped or with a small remaining velocity magnitude. The participants controlled the Cartesian x, z, $pitch$ and yaw velocities of the robot end-effector, in the end-effector local frame. The arm was reset to the initial position if any part of the robot collided with the environment, the physical model of the user, or any of the target cans. The participant would then loose the time spent up until the collision, as the timer kept running. For all trials the participants were instructed to attempt to achieve the lowest mean times possible, while keeping in mind that collisions were costly in terms of time.

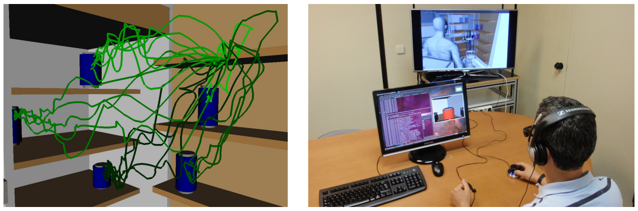

(a) Example translational trajectories. Partic. 6, shared control.

(b) Participant performing experiment (with 3D effects activated).

Fig. 8. The experiment setup.

D. Physical Setup

The physical experiment setup can be seen in Fig. 8(b). The input device was a SpaceNavigator 6 DOF joystick. The simulation of the robot in the environment was displayed in 3D on a 40 inch (approx. 102 cm) display (Samsung 3D TV, UE40D8000). The participants used active 3D glasses. This gave some perception of the depth of the scene. On a smaller display closer to the participant the end-effector camera view was shown. See Fig. 12. The physical size of the camera image was comparable to a commercial tablet computer. A colored timer was also shown.

E. Procedure

The testing was performed over 2 days for each participant, with multiple sessions each day. The total time

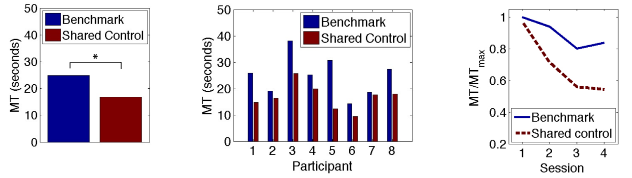

(a) Average MT over participants.

(b) Individual MT for each participant.

(c) Average MT learning curves.

Fig. 9. The Mean Time (MT) with and without (benchmark condition) the shared control. Based on the two non-training sessions for each condition.

committed each day was about one hour per participant. Each session consisted of 3 repetitions of each of the 5 tasks (5 target locations), for 15 trials in total. The first day the participants were introduced to the experimental setup and was given 3 sessions for training. This was followed by 2 sessions for establishing a benchmark. The shared control was not used. The second day the participants were introduced to the shared control, and were first given a maximum of 2 training sessions with the adaptive shared control activated. That is, each participant was told to attempt to achieve a comfortable level of assistance, and could decide when the training should be ended. Then the adaptation was disabled, and each participant was given 2 sessions to establish the performance with the shared control, using the previously learned neural network weights.

IV. RESULTS AND DISCUSSION

The overall results, expressed in Mean Time (MT), can be seen in Fig. 9. There was a statistically significant improvement in average MT over participants of 32.5% with the shared control. A paired t-test was used, with $t(7) = 3.96$, $p = 0.005$. This is comparable to previous work [7]. Fig. 9(b) shows the equivalent comparison for each participant. While all participants had a reduction in the MT metric, there were large individual differences in the amount of reduction, ranging from 5.3% for participant 7 to 59.9% for participant 5. It is interesting that both the fastest (participant 6) and the slowest (participant 3) for both conditions had improvements of over 30%, given the very different abilities of the two participants. That is, in under 20 minutes each participant was able to "negotiate" a level of assistance that at least did not inhibit the performance, and for most cases seems to have improved the performance. See Fig. 10 for examples of the development of the neural network weights for the final link. A system with a static level of assistance could easily become another obstacle to overcome for the user. A corresponding visualization of the final usage of the proximity sensors is given in Fig. 11. While participant 3 primarily received assistance when close to obstacles on the left, participants 5 and 6 had a more symmetric usage of the proximity sensors. The latter two participants also used the in-hand sensors, which are useful for slowing the robot down in the last moments of the tasks. An example of the effect of the shared control on the end-effector velocities can be seen in Fig. 12. Significant assistance is provided as the participant is approaching the target can, by the limitation of the commanded x and z velocities from 12 seconds onwards. It can also be seen that the system allows the user to freely perform gross movements when there is sufficient space (first 4 seconds here).

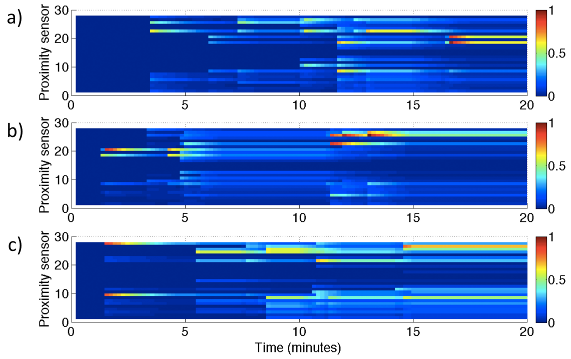

Fig. 10. Examples of the development of the neural network weights for the final link. Mean weights for each proximity sensor of final link, normalized with maximum over 3 participants: a) 3, b) 5 and c) 6.

Given the within-subject experiment design and steep learning curve on the tasks performed, extensive practice was needed before measuring performance. Fig. 9(c) shows that the MT improved considerably during the first 2 sessions for each condition and stabilized reasonably well for the last 2 sessions (in which performance was measured). Furthermore, to avoid excessive fatigue in the participants the experiment was spread over 2 days. There is extensive evidence of the enhancing effect of sleep on motor sequence learning in sequential finger tapping tasks. On tasks more similar to the one used here, like pursuit tracking, there is less evidence of a significant effect [19]. Future experiments should attempt to minimize this risk by performing training, benchmarking and shared control on separate days, with counterbalancing.

V. CONCLUSIONS AND FUTURE WORK

An adaptive collision-limitation behavior for assistive manipulators was developed. The approach has several interesting features with respect to previous work in shared control. It can be applied to high-DOF manipulator platforms operating in environments where a set of sufficiently accurate environment models and sensor to end-effector mappings are difficult to obtain. In addition, the adaptation is performed

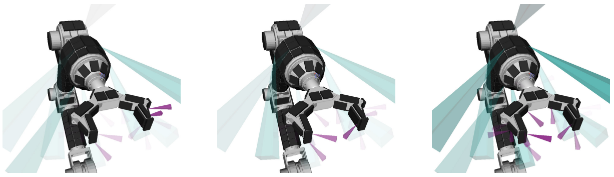

(a) Participant 3.

(b) Participant 5.

(c) Participant 6.

Fig. 11. Visualizations of the learned proximity sensor usage for the final link. Transparency of square pyramid representing the field of view of a given sensor is made to vary with the mean neural network weights for sensor. High transparency indicates low usage, and vice versa.

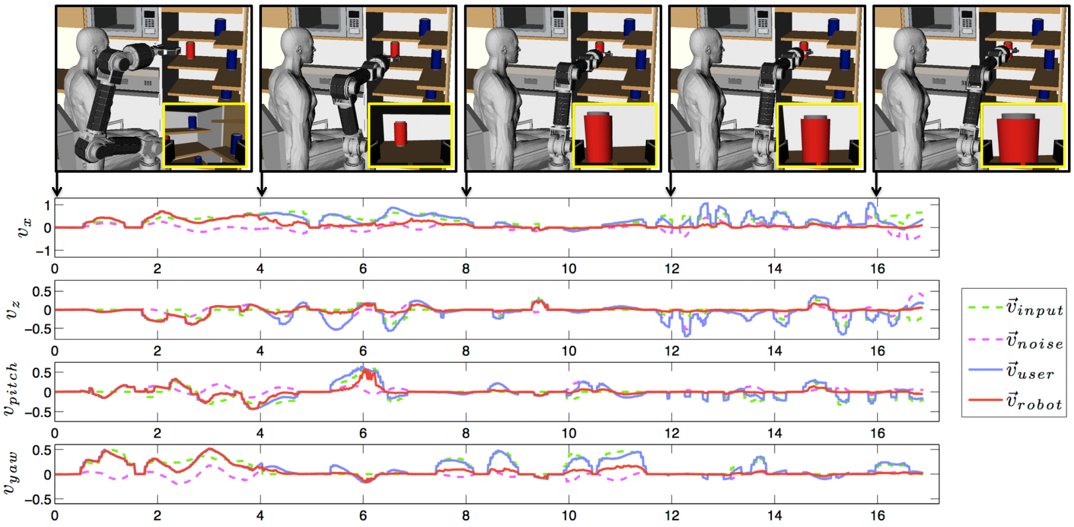

Fig. 12. One attempt by participant 1 on task 3 with shared control. Cartesian x, z, $pitch$ and yaw components of velocities (in end-effector frame) shown, with time in seconds on the x-axis. A discrepancy between the input ($\vec{v}_{user}$) and the output ($\vec{v}_{robot}$) velocities of the shared control means assistance is provided. Actual robot poses along trajectory shown, but the camera angle is altered for visualization. End-effector camera view shown in inserts. Description of phases: 0-4 seconds: highly coordinated gross movement, 4-8 seconds: adjustment of pitch during forward movement, 8-12 seconds: mainly yaw adjustments, 12-16 seconds: the final approach to the target.

online using an unsupervised Hebbian learning by associating a distributed set of proximity sensors with experienced collisions. A controlled experiment with realistic simulations of the tasks, sensors and the 5 DOF ASIBOT manipulator showed promising results for 8 able-bodied participants with simulated disabilities. Future work should aim to improve the experimental paradigm used, and explore the application on a larger set of tasks and to usage over a longer time-frame. How well the learned neural network weights can generalize to different tasks should also be investigated.

VI. ACKNOWLEDGMENTS

Funding has been received from the ARCADIA project DPI2010-21047-C02-0, thanks to the MINECO ministry of Spain, and the ROBOCITY2030 II project S2009/DPI-1559, thanks to Comunidad de Madrid and EU structural funds.

REFERENCES

[1] A. Jardón, A. Giménez, R. Correal, R. Cabas, S. Martínez and C. Balaguer, A portable light-weight climbing robot for personal assistance applications, *Industrial Robot: An International Journal*, vol. 33. no. 4, pp. 303-307, 2006.

[2] G. Vanacker, D. Vanhooydonck, E. Demeester, A. Huntemann, A. Degeest, and H. Brussel, "Adaptive filtering approach to improve wheelchair driving performance", *in ROMAN 2006 - The 15th IEEE International Symposium on Robot and Human Interactive Communication*, Hatfield, United Kingdom, 2006, pp. 527-532.

[3] E. Demeester, A. Huntemann, D. Vanhooydonck, G. Vanacker, H. Brussel and M. Nuttin, User-adapted plan recognition and user-adapted shared control: A bayesian approach to semi-autonomous wheelchair driving, *Journal of Autonomous Robots*, vol. 24, pp. 193-211, 2008.

[4] T. Carlson and Y. Demiris, "Human-wheelchair collaboration through prediction of intention and adaptive assistance", *in IEEE Int. Conf. on Robotics and Automation*, Pasadena, CA, 2008, pp. 3926-3931.

[5] M.A. Goodrich, D.R. Olsen, J.W. Crandall and T.J. Palmer, "Experiments in adjustable autonomy", *in Proceedings of IJCAI Workshop on Autonomy, Delegation and Control: Interacting with Intelligent Agents*, 2001, pp. 1624-1629.

[6] B. Pitzer, M. Styer, C. Bersch, C. DuHadway and J. Becker, "Towards Perceptual Shared Autonomy for Robotic Mobile Manipulation", *in Proceedings of IEEE International Conference on Robotic and Automation*, Shanghai, China, 2011, pp. 6245-6251.

[7] M.F. Stoelen, V.F. Tejada, A. Jardón, F. Bonsignorio and C. Balaguer, "Benchmarking Shared Control for Assistive Manipulators: From Controllability to the Speed-Accuracy Trade-Off", *in Proceedings of the IEEE/RSJ International Conference on Intelligent Robots and Systems*, Vilamoura, Portugal, 2012, pp. 4386-4391.

[8] G. Cannata, M. Maggiali, G. Metta and G. Sandini, "An Embedded Artificial Skin for Humanoid Robots", *in Proceedings of the IEEE International Conference on Multisensor Fusion and Integration for Intelligent Systems*, Seoul, Korea, 2008.

[9] E. Cheung and V.J. Lumelsky, Proximity sensing in robot manipulator motion planning: system and implementation issues, *IEEE Transactions on Robotics and Automation*, vol. 5, no. 5, 1989, pp. 740-751.

[10] K. Hsiao, P. Nangeroni, M. Huber, A. Saxena and A.Y. Ng, "Reactive grasping using optical proximity sensors", *in IEEE Int. Conf. on Robotics and Automation*, Kobe, Japan, 2009, pp. 2098-2105.

[11] H. Yousef, M. Boukallel and K. Althoefer, Tactile sensing for dexterous in-hand manipulation in robotics - A review, *Sensors and Actuators A: Physical*, vol. 167, no. 2, pp. 171-187, 2011.

[12] R. Pfeifer and C. Scheier, *Understanding Intelligence*, MIT Press, Cambridge, MA; 1999.

[13] R. Diankov, Automated Construction of Robotics Manipulation Programs, *PhD thesis*, Robotics Institute, Carnegie Mellon University, Aug. 2010.

[14] K.M. Tsui and H.A. Yanco, "Towards Establishing Clinical Credibility for Rehabilitation and Assistive Robots Through Experimental Design", *in Workshop on Good experimental methodology in robotics, Robotics Science and Systems*, Seattle, WA, USA, 2009.

[15] J. Mankoff, H. Fait and R. Juang, Evaluating accessibility by simulating the experiences of users with vision or motor impairments, *IBM Systems Journal*, vol. 44, no. 3, pp. 505-517, 2005.

[16] A.A. Faisal, L.P.J. Selen and D.M. Wolpert, Noise in the nervous system, *Nat. Rev. Neurosci.*, vol. 9, no. 4, pp. 292-303, 2008.

[17] P.H. McCrea and J.J. Eng, Consequences of increased neuromotor noise for reaching movements in persons with stroke, *Exp. Brain Res.*, vol 162, pp. 70-77, 2005.

[18] T.D. Sanger, J. Kaiser and B. Placek, Reaching Movements in Childhood Dystonia Contain Signal-Dependent Noise, *Journal of Child Neurology*, vol. 20, no. 6, pp. 489-496, 2005.

[19] K. Blischke, D. Erlacher, H. Kresin, S. Brueckner and A. Malangré, "Benefits of Sleep in Motor Learning - Prospects and Limitations", *Journal of Human Kinetics*, vol. 20, pp. 23-35, 2008.